Measurement of the νe−nucleus charged-current double-differential cross section at ⟨Eν⟩ = 2.4 GeV using NOvA

Article (Published Version)

Measurement of the ν_e-Nucleus Charged-Current Double-Differential Cross Section at $\langle E_\nu \rangle = 2.4$ GeV Using NOvA

M. A. Acero,[2] P. Adamson,[12] L. Aliaga,[12] N. Anfimov,[25] A. Antoshkin,[25] E. Arrieta-Diaz,[27] L. Asquith,[39] A. Aurisano,[6] A. Back,[19,23] M. Baird,[19,39,44] N. Balashov,[25] P. Baldi,[24] B. A. Bambah,[16] S. Bashar,[42] K. Bays,[4,18] R. Bernstein,[12] V. Bhatnagar,[33] D. Bhattarai,[31] B. Bhuyan,[14] J. Bian,[24,30] A. C. Booth,[35,39] R. Bowles,[19] B. Brahma,[17] C. Bromberg,[28] N. Buchanan,[8] A. Butkevich,[21] S. Calvez,[8] T. J. Carroll,[41,47] E. Catano-Mur,[46] S. Childress,[12] A. Chatla,[16] R. Chirco,[18] B. C. Choudhary,[10] A. Christensen,[8] T. E. Coan,[38] M. Colo,[46] L. Cremonesi,[35] G. S. Davies,[31,19] P. F. Derwent,[12] P. Ding,[12] Z. Djurcic,[1] M. Dolce,[42] D. Doyle,[8] D. Dueñas Tonguino,[6] E. C. Dukes,[44] R. Ehrlich,[44] M. Elkins,[23] E. Ewart,[19] G. J. Feldman,[48] P. Filip,[22] J. Franc,[9] M. J. Frank,[36] H. R. Gallagher,[42] R. Gandrajula,[28,44] F. Gao,[34] A. Giri,[17] R. A. Gomes,[13] M. C. Goodman,[1] V. Grichine,[26] M. Groh,[8,19] R. Group,[44] B. Guo,[37] A. Habig,[29] F. Hakl,[20] A. Hall,[44] J. Hartnell,[39] R. Hatcher,[12] H. Hausner,[47] M. He,[15] K. Heller,[30] V. Hewes,[6] A. Himmel,[12] B. Jargowsky,[24] J. Jarosz,[8] F. Jediny,[9] C. Johnson,[8] M. Judah,[8,34] I. Kakorin,[25] D. M. Kaplan,[18] A. Kalitkina,[25] R. Keloth,[7] O. Klimov,[25] L. W. Koerner,[15] L. Kolupaeva,[25] S. Kotelnikov,[26] R. Kralik,[39] Ch. Kullenberg,[25] M. Kubu,[9] A. Kumar,[33] C. D. Kuruppu,[37] V. Kus,[9] T. Lackey,[12,19] K. Lang,[41] P. Lasorak,[39] J. Lesmeister,[15] S. Lin,[8] A. Lister,[47] J. Liu,[24] M. Lokajicek,[22] J. M. C. Lopez,[43] R. Mahji,[16] S. Magill,[1] M. Manrique Plata,[19] W. A. Mann,[42] M. T. Manoharan,[7] M. L. Marshak,[30] M. Martinez-Casales,[23] V. Matveev,[21] B. Mayes,[39] M. D. Messier,[19] H. Meyer,[45] T. Miao,[12] V. Mikola,[43] W. H. Miller,[30] S. Mishra,[3] S. R. Mishra,[37] A. Mislivec,[30] R. Mohanta,[16] A. Moren,[29] A. Morozova,[25] W. Mu,[12] L. Mualem,[4] M. Muether,[45] K. Mulder,[43] D. Naples,[34] A. Nath,[14] N. Nayak,[24] S. Nelleri,[7] J. K. Nelson,[46] R. Nichol,[43] E. Niner,[12] A. Norman,[12] A. Norrick,[12] T. Nosek,[5] H. Oh,[6] A. Olshevskiy,[25] T. Olson,[42] J. Ott,[24] A. Pal,[32] J. Paley,[12] L. Panda,[32] R. B. Patterson,[4] G. Pawloski,[30] O. Petrova,[25] R. Petti,[37] D. D. Phan,[41,43] R. K. Plunkett,[12] A. Pobedimov,[25] J. C. C. Porter,[39] A. Rafique,[1] L. R. Prais,[31] V. Raj,[4] M. Rajaoalisoa,[6] B. Ramson,[12] B. Rebel,[12,47] P. Rojas,[8] P. Roy,[45] V. Ryabov,[26] O. Samoylov,[25] M. C. Sanchez,[23] S. Sánchez Falero,[23] P. Shanahan,[12] S. Shukla,[3] A. Sheshukov,[25] I. Singh,[10] P. Singh,[35,10] V. Singh,[3] E. Smith,[19] J. Smolik,[9] P. Snopok,[18] N. Solomey,[45] A. Sousa,[6] K. Soustruznik,[5] M. Strait,[30] L. Suter,[12] A. Sutton,[44] S. Swain,[32] C. Sweeney,[43] A. Sztuc,[43] R. L. Talaga,[1] B. Tapia Oregui,[41] P. Tas,[5] B. N. Temizel,[18] T. Thakore,[6] R. B. Thayyullathil,[7] J. Thomas,[43,47] E. Tiras,[11,23] J. Tripathi,[33] J. Trokan-Tenorio,[46] Y. Torun,[18] J. Urheim,[19] P. Vahle,[46] Z. Vallari,[4] J. Vasel,[19] T. Vrba,[9] M. Wallbank,[6] T. K. Warburton,[23] M. Wetstein,[23] D. Whittington,[40,19] D. A. Wickremasinghe,[12] T. Wieber,[30] J. Wolcott,[42] W. Wu,[24] Y. Xiao,[24] B. Yaeggy,[6] A. Yallappa Dombara,[40] A. Yankelevich,[24] K. Yonehara,[12] S. Yu,[1,18] Y. Yu,[18] S. Zadorozhnyy,[21] J. Zalesak,[22] Y. Zhang,[39] and R. Zwaska[12]

(NOvA Collaboration)

[1]*Argonne National Laboratory, Argonne, Illinois 60439, USA*
[2]*Universidad del Atlantico, Carrera 30 No. 8-49, Puerto Colombia, Atlantico, Colombia*
[3]*Department of Physics, Institute of Science, Banaras Hindu University, Varanasi 221 005, India*
[4]*California Institute of Technology, Pasadena, California 91125, USA*
[5]*Charles University, Faculty of Mathematics and Physics, Institute of Particle and Nuclear Physics, Prague, Czech Republic*
[6]*Department of Physics, University of Cincinnati, Cincinnati, Ohio 45221, USA*
[7]*Department of Physics, Cochin University of Science and Technology, Kochi 682 022, India*
[8]*Department of Physics, Colorado State University, Fort Collins, Colorado 80523-1875, USA*
[9]*Czech Technical University in Prague, Brehova 7, 115 19 Prague 1, Czech Republic*
[10]*Department of Physics and Astrophysics, University of Delhi, Delhi 110007, India*
[11]*Department of Physics, Erciyes University, Kayseri 38030, Turkey*
[12]*Fermi National Accelerator Laboratory, Batavia, Illinois 60510, USA*
[13]*Instituto de Física, Universidade Federal de Goiás, Goiânia, Goiás 74690-900, Brazil*
[14]*Department of Physics, IIT Guwahati, Guwahati 781 039, India*
[15]*Department of Physics, University of Houston, Houston, Texas 77204, USA*
[16]*School of Physics, University of Hyderabad, Hyderabad 500 046, India*
[17]*Department of Physics, IIT Hyderabad, Hyderabad 502 205, India*
[18]*Illinois Institute of Technology, Chicago Illinois 60616, USA*
[19]*Indiana University, Bloomington, Indiana 47405, USA*
[20]*Institute of Computer Science, The Czech Academy of Sciences, 182 07 Prague, Czech Republic*
[21]*Institute for Nuclear Research of Russia, Academy of Sciences 7a, 60th October Anniversary prospect, Moscow 117312, Russia*

[22]Institute of Physics, The Czech Academy of Sciences, 182 21 Prague, Czech Republic
[23]Department of Physics and Astronomy, Iowa State University, Ames, Iowa 50011, USA
[24]Department of Physics and Astronomy, University of California at Irvine, Irvine, California 92697, USA
[25]Joint Institute for Nuclear Research, Dubna, Moscow region 141980, Russia
[26]Nuclear Physics and Astrophysics Division, Lebedev Physical Institute, Leninsky Prospect 53, 119991 Moscow, Russia
[27]Universidad del Magdalena, Carrera 32 No 22-08 Santa Marta, Colombia
[28]Department of Physics and Astronomy, Michigan State University, East Lansing, Michigan 48824, USA
[29]Department of Physics and Astronomy, University of Minnesota Duluth, Duluth, Minnesota 55812, USA
[30]School of Physics and Astronomy, University of Minnesota Twin Cities, Minneapolis, Minnesota 55455, USA
[31]University of Mississippi, University, Mississippi 38677, USA
[32]National Institute of Science Education and Research, Khurda 752050, Odisha, India
[33]Department of Physics, Panjab University, Chandigarh 160 014, India
[34]Department of Physics, University of Pittsburgh, Pittsburgh, Pennsylvania 15260, USA
[35]Particle Physics Research Centre, Department of Physics and Astronomy, Queen Mary University of London, London E1 4NS, United Kingdom
[36]Department of Physics, University of South Alabama, Mobile, Alabama 36688, USA
[37]Department of Physics and Astronomy, University of South Carolina, Columbia, South Carolina 29208, USA
[38]Department of Physics, Southern Methodist University, Dallas, Texas 75275, USA
[39]Department of Physics and Astronomy, University of Sussex, Falmer, Brighton BN1 9QH, United Kingdom
[40]Department of Physics, Syracuse University, Syracuse New York 13210, USA
[41]Department of Physics, University of Texas at Austin, Austin, Texas 78712, USA
[42]Department of Physics and Astronomy, Tufts University, Medford, Massachusetts 02155, USA
[43]Physics and Astronomy Department, University College London, Gower Street, London WC1E 6BT, United Kingdom
[44]Department of Physics, University of Virginia, Charlottesville, Virginia 22904, USA
[45]Department of Mathematics, Statistics, and Physics, Wichita State University, Wichita, Kansas 67206, USA
[46]Department of Physics, William & Mary, Williamsburg, Virginia 23187, USA
[47]Department of Physics, University of Wisconsin-Madison, Madison, Wisconsin 53706, USA
[48]Department of Physics, Harvard University, Cambridge, Massachusetts 02138, USA

(Received 6 July 2022; revised 13 September 2022; accepted 8 November 2022; published 3 February 2023)

The inclusive electron neutrino charged-current cross section is measured in the NOvA near detector using 8.02×10^{20} protons-on-target in the NuMI beam. The sample of GeV electron neutrino interactions is the largest analyzed to date and is limited by $\simeq$17% systematic rather than the $\simeq$7.4% statistical uncertainties. The double-differential cross section in final-state electron energy and angle is presented for the first time, together with the single-differential dependence on Q^2 (squared four-momentum transfer) and energy, in the range 1 GeV $\leq E_\nu <$ 6 GeV. Detailed comparisons are made to the predictions of the GENIE, GiBUU, NEUT, and NuWro neutrino event generators. The data do not strongly favor a model over the others consistently across all three cross sections measured, though some models have especially good or poor agreement in the single differential cross section vs Q^2.

DOI: 10.1103/PhysRevLett.130.051802

Precision measurements of neutrino oscillation parameters [1–4] such as δ_{CP} and the neutrino mass ordering use ν_e ($\bar{\nu}_e$) appearance in predominantly ν_μ ($\bar{\nu}_\mu$) beams and depend on detailed understanding of neutrino interaction models. Despite the two-detector technique that largely mitigates the impact of cross-section uncertainties, oscillation measurements still require model predictions to estimate the energy spectrum and selection efficiencies of ν_e interactions via accurate modeling of interaction rate and outgoing-particle kinematics.

Lepton universality suggests that ν_μ and ν_e interactions are largely similar, but differences in final-state lepton mass, tree-level radiative corrections, and imprecisely known form factors of the nucleon lead to differences in the predicted cross sections and their uncertainties [5]. There are few direct ν_e cross-section measurements at the GeV energy scale as ν_e comprise $\leq 1\%$ of the neutrino beams produced at accelerators. The dominant ν_μ component produces significant backgrounds. Previous measurements in this energy range have been performed by Gargamelle [6] and T2K [7,8], both of which reported the total integrated cross section as a function of energy. MINERvA has reported single-differential cross sections

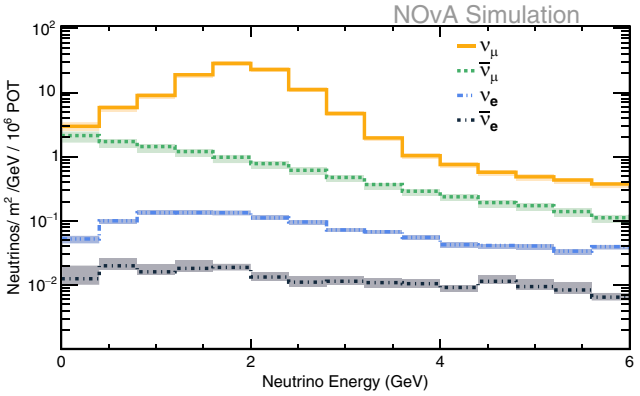

FIG. 1. NuMI neutrino-mode beam flux spectra at the NOvA ND below 6 GeV. The bands represent the total flux uncertainty on hadron production and beam optics for each component.

for the quasielastic component of the ν_e—carbon cross section [9]. The measurement presented here uses the largest GeV sample of electron neutrino-initiated interactions to date, with which the simultaneous differential dependence on electron energy E_e and angle θ_e is extracted for the first time. The cross sections as functions of squared four-momentum transfer Q^2 and neutrino energy E_ν are also presented.

Generators, such as [10–13], group predictions of neutrino-nucleus interaction cross sections into three processes in this energy range: quasielastic (QE), baryon resonance production (RES), and deep inelastic scattering (DIS). The modeling of these processes must be altered in the nuclear medium. A fourth process due to meson exchange current (MEC) occurs only inside the nuclei. These nuclear effects are not completely understood and the implementation of existing models in generators is currently incomplete [14–17]. Measured differential dependencies using ν_e can be used to constrain the underlying interaction channels, elucidate nuclear effects, and probe key aspects of neutrino-nucleus interaction models used to calculate oscillation-experiment acceptances.

The NOvA experiment is designed to measure neutrino flavor oscillations [1] using two detectors separated by 809 km, placed 14.6 mrad off axis from the central beam direction of Fermilab's NuMI beam [18]. Magnetic focusing horns in the beamline charge-select neutrino parents giving 96% ν_μ flux between 1 and 6 GeV. The energy spectrum peak at 1.8 GeV at the near detector (ND) as shown in Fig. 1. The largest contamination is $\bar{\nu}_\mu$; the $<1\%$ $\nu_e + \bar{\nu}_e$ arises mostly from muon decays below 3 GeV neutrino energy and kaon decays above.

The ND is a tracking calorimeter composed of liquid scintillator-filled PVC cells. The portion of the detector relevant to this measurement is 3.9 m × 3.9 m × 12.8 m (long dimension along beam direction) in size and is segmented into cells 3.9 m long with a rectangular cross section of 6.6 cm (0.15 radiation length) in the beam direction and 3.9 cm (0.45 Molière radius) transverse to the beam, spanning the height and width of the detector in planes of alternating vertical and horizontal orientation. Each cell is filled with a blend of 95% mineral oil and 5% pseudocumene with trace concentrations of wavelength shifting fluors [19]. The resulting composition by mass is 67% carbon, 16% chlorine, 11% hydrogen, 3% titanium, and 3% oxygen with other trace elements. When a particle traverses the detector, a wavelength-shifting fiber in the cell collects and delivers scintillation light to an avalanche photodiode. The result is digitized by custom front-end electronics. All signals above a noise-vetoing threshold are sent to a data buffer.

This Letter presents data corresponding to 8.02×10^{20} protons delivered to the NuMI production target (POT) between November 2014 and February 2017.

This analysis relies on simulation to calculate the flux, optimize event selection criteria, estimate selection efficiency, and assess the effects of detector resolution, acceptance, and systematic uncertainties. The simulation proceeds in several steps: first neutrinos are generated from simulated mesons in the NuMI beam, then those neutrinos interact with nuclei in the detector, after which the final-state particles are transported through the detector.

The NuMI flux is predicted using GEANT4 v9.03 [20] with the FTFP BERT hadronic model. The hadron production model is adjusted and constrained using external measurements by the PPFX package [21]. Neutrino interactions are simulated using the GENIE v2.12.2 [10] event generator, hereinafter referred to as GENIE v2. The neutrino-interaction model output is adjusted to incorporate advances in theory and external data to better match a sample of ν_μ charged-current (CC) interactions from NOvA ND data as detailed in Ref. [22]. In this dedicated tune, hereinafter referred to as the NOvA tune, there are three substantial adjustments to the GENIE v2 prediction: (1) the QE axial mass (M_A CCQE) is changed from 0.99 to 1.04 GeV/c^2 [23]; (2) soft non-resonant single pion production events from neutrinos are reduced by 57%; (3) the empirical MEC model [24] is tuned to ND data using a two-dimensional fit in hadronic energy and momentum transfer. This procedure changes the shape of the MEC prediction and increases its cross section by 50%. The NOvA-tune is applied to all simulated CC interactions.

GEANT4(v10.1.p3) is used to simulate energy deposited in the NOvA ND from the particles generated by neutrino interactions. Photon generation and propagation are modeled separately as follows: (1) the modeling and transfer of scintillation light uses NOvA measurements of scintillator response and fiber attenuation properties [25]; (2) the Birks suppression of the scintillation light is tuned using test-stand measurements and validated using a custom simulated response of the readout electronics [26].

The signature of ν_e CC interactions is an electron in the final state that produces an electromagnetic cascade within

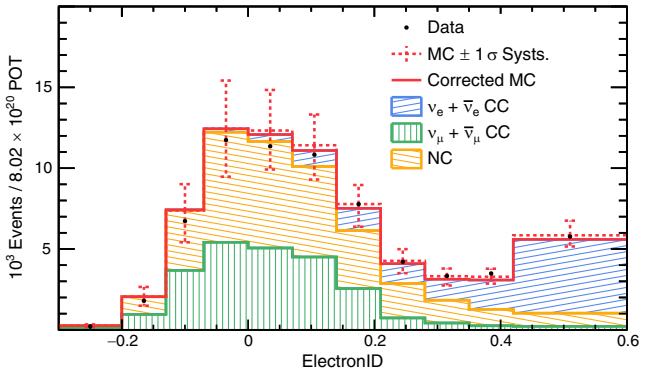

FIG. 2. Simulated ElectronID distributions of $\nu_e + \bar{\nu}_e$ CC (blue), $\nu_\mu + \bar{\nu}_\mu$ CC (orange), and NC (green), compared to data integrated over the reported electron kinematic phase space. The dashed (solid) line shows the total prediction from simulation (after extracted fit normalization corrections). Statistical uncertainties on data are too small to be seen. The vertical errors represents the $\pm 1\sigma$ systematic range. All spectra are normalized to the data exposure.

the detector. The major backgrounds are neutral current (NC) and ν_μ CC interactions with final-state π^0s that decay into two photons. These can mimic electron energy depositions if the showers overlap or one photon is low energy.

Candidate neutrino interactions (events) are reconstructed by forming collections of observed energy deposits (hits) from final-state charged particles correlated in space and time [27]. Events are assigned a vertex by minimizing the angular spread of hits relative to candidate vertices [28]. Using a fuzzy K-means algorithm, hits within the event are clustered in regions of space emanating from the vertex into reconstructed particle trajectories (prongs) [29]. Primary event vertices are required to be contained in a 49 t fiducial volume spanning 2.8 m in both width and height and 6.5 m in length. All prongs are required to stop at least 30 cm from any edge of the detector to ensure containment. Events containing between 20 and 200 hits and at least one prong are selected for analysis. Events outside this range are generally low visible energy NC events or high-multiplicity events in which the electromagnetic cascade is difficult to isolate.

Prongs are identified as candidate electrons using a boosted decision tree (BDT) algorithm [30]. One input to the BDT is the output of a convolutional neural network trained using simulated samples of single particles labeling prongs as muonic, electromagnetic, or hadronic in origin. Other inputs include the energy-weighted transverse width of the prong and the distance from the vertex to the prong start aiding the separation of photon- from electron-induced showers. BDT performance was validated against a sideband of data enriched with EM showers in $\nu_\mu \mathrm{CC}\pi^0$ events. Candidate events are assigned an ElectronID score equal to the most electron-like BDT score of their constituent prongs. Figure 2 shows the ElectronID distribution in data and simulation after selection criteria (and kinematic restrictions, defined below) are applied.

The selected sample is binned according to the candidate electron shower's calorimetric energy E_e, and angle $\cos\theta_e$. Within each electron kinematic bin, the simulated ElectronID distribution is used to generate signal and background predictions, or templates. Each bin's templates are broken further into three components, whose three independent normalization parameters are constrained in a simultaneous fit to the data: $\nu_e + \bar{\nu}_e$, $\nu_\mu + \bar{\nu}_\mu$, and NC. Neutrinos and antineutrinos are not separated due to similarities in the shapes of their templates.

Electron-kinematic bins that satisfy two criteria are included in the fit: at least 100 predicted signal events and an estimated signal-to-background ratio > 0.4 in the ElectronID > 0.2 region. These requirements remove regions (e.g., $\cos\theta_e > 0.94, 1 \leq E_e < 1.5$ GeV) that do not have adequate discrimination between signal and photon-induced backgrounds and limit the measurement to the kinematic ranges:

$$\begin{aligned} &0.85 \leq \cos\theta_e < 0.90 \cap 1.0 \leq E_e(\mathrm{GeV}) < 1.65, \\ &0.90 \leq \cos\theta_e < 0.94 \cap 1.0 \leq E_e(\mathrm{GeV}) < 2.0, \\ &0.94 \leq \cos\theta_e < 0.97 \cap 1.4 \leq E_e(\mathrm{GeV}) < 3.0, \\ &0.97 \leq \cos\theta_e \leq 1.00 \cap 1.4 \leq E_e(\mathrm{GeV}) < 6.0. \end{aligned} \quad (1)$$

A χ^2 minimization procedure [31] fits the normalizations of the signal and two background templates. A covariance matrix encodes the correlations between templates across all kinematic and template bins using systematic uncertainties which affect the shape of ElectronID and reconstructed electron kinematics within the fit. The fit produces a χ^2 of 131 for 141 degrees of freedom and normalization parameters ranging between 0.9 to 1.1 with outliers in low-statistics, high-uncertainty bins. A sample purity of $13 \pm 1.3\%$ is predicted by extracting signal and background as the integral of the corresponding post-fit templates. Uncertainties on purity rise to 1.5% in kinematic regions where the $\nu_\mu + \bar{\nu}_\mu$ and NC normalization parameters are highly correlated due to similarities in template shape. The contribution of $\bar{\nu}_e$ CC background is removed from the renormalized signal template using the 5% contribution from simulation. The resulting sample is estimated to contain 9200 ± 1000 ν_e CC interaction candidates. The selection efficiency is approximately 40% at 2 GeV, $\cos\theta_e \geq 0.97$ and reduces linearly to 13% at the edges of the phase space with an average of 23%. The signal sample is estimated to be 28% QE, 20% MEC, 31% RES, 20% DIS, and 1% CC coherent pion production.

The flux-averaged double-differential ν_e CC cross section in final state electron kinematic variables is constructed using

TABLE I. Fractional uncertainties and correlations, broken down by source. Averages are taken across all reported bins, weighted by the measured cross section.

Source	Average uncertainty (%)	Average correlation
Flux	10.3	0.90
ν-A model	9.8	0.64
Calibration	5.9	0.05
Detector model	5.6	0.21
Other	2.8	0.03
Statistical	7.4	0.02
Total	18.2	0.59

$$\left(\frac{d^2\sigma}{d\cos\theta dE}\right)_i = \frac{\sum_j U_{ij}^{-1} N_{\nu_e}(\cos\theta, E)_j}{N_t \phi \epsilon(\cos\theta, E)_i \Delta\cos\theta_i \Delta E_i}, \quad (2)$$

where N_{ν_e} is the estimated ν_e CC events from the template fit. U_{ij} is an unfolding matrix used to relate the reconstructed value in bin j to the true value in bin i. The data are iteratively unfolded using d'Agostini's method [32] with two iterations as implemented in RooUnfold [33]. The optimal number was found by minimizing the average mean square error [34] calculated across simulated samples with random variations of systematic uncertainties. N_t is the number of nuclear targets in the fiducial volume, ϕ the integrated neutrino flux, ϵ the selection efficiency correction factor, and ΔE and $\Delta\cos\theta$ are the bin widths used for the electron kinematic variables. Bin widths are chosen small enough to match the detector resolution and large enough to include a statistically significant event sample. The average E_e resolution is 350 MeV, and the angular resolution ranges from 2° for forward-going electrons to 11° for less forward-going electrons.

Table I summarizes the effects of sources of uncertainty on the measurements. Systematic uncertainties are evaluated by varying the parameters used to model neutrino flux, neutrino-nucleus interactions (ν-A), detector response, and re-extracting the differential cross section. The difference between the cross section extracted using the nominal simulation and that extracted using the simulation with a varied parameter is taken as the uncertainty due to each parameter. The procedure accounts for changes in the compositions of backgrounds, selection efficiency, and event reconstruction due to the variations considered.

Dominant sources of systematic uncertainty are from the neutrino flux and ν-A predictions. Uncertainties on the flux arise from hadron production uncertainties (9%) [21] and beam optics modeling (4%). ν-A modeling uncertainties are assessed through reweightable parameters from the GENIE generator [10] and a custom set of NOvA-specific uncertainties [22]. At $E_\nu < 3$ GeV, parameters affecting the RES signal and backgrounds (CC/NCπ^0) and the MEC signal prediction are dominant. DIS related multipion production uncertainties dominate at $E_\nu > 3$ GeV.

Nonleading sources of uncertainty come from detector calibration and modeling. These sources become dominant at $\cos\theta_e < 0.94$ and $E_e < 1.5$ GeV. Minor sources of uncertainty, which include detector mass, integrated beam exposure, beam intensity modeling, and the modeling of diffractive (DFR) π^0 production, are combined in the "other" category of Table I. DFR modeling uncertainties are evaluated by reweighting the default ν-H NC interactions producing a π^0 prediction from GENIE to an estimate based on the Kopeliovich model *et al.* [35,36] as a function of E_ν and the Björken scaling variables. The average uncertainty on DFR modeling is 2.6%.

Table I shows the weighted average bin-to-bin correlations [37] calculated as

$$\langle \text{corr} \rangle = \frac{\sum_{i<j} C_{ij} \times \sigma_i \times \sigma_j}{\sum_{i<j} \sigma_i \times \sigma_j}, \quad (3)$$

where C_{ij} is the correlation between bins i and j and σ_i is the double-differential cross section measured in bin i for each source of systematic uncertainty. Large average correlation from the flux uncertainty indicate that it mainly impacts normalization. Interaction modeling also exhibits strong correlations across all bins, due to a combination of the template fitting procedure and model parameters, such as the axial mass from the RES model and DIS pion production uncertainties, that impact selection efficiency.

Three results are presented: the flux-integrated double-differential cross section vs electron energy and angle shown in Fig. 3, the cross section vs E_ν shown in Fig. 4,

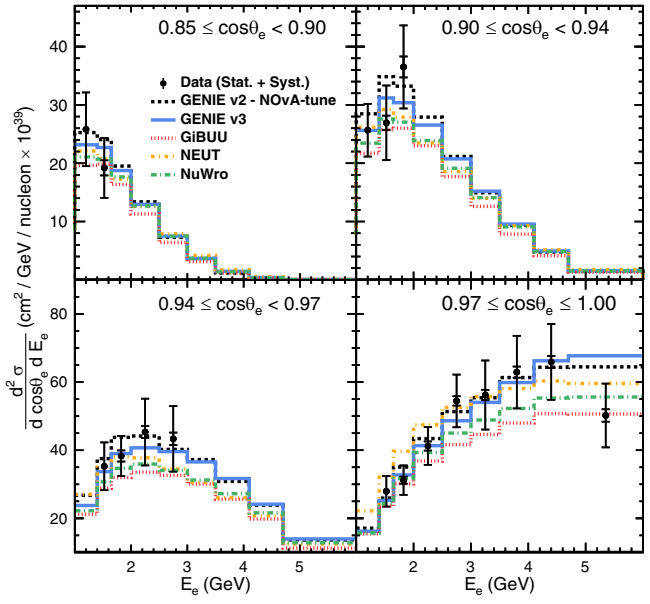

FIG. 3. Extracted double differential cross section, subdivided in slices of electron angle. The outer error bars of the data represent total uncertainties, while the inner error bars are statistical only. The data are compared to several models.

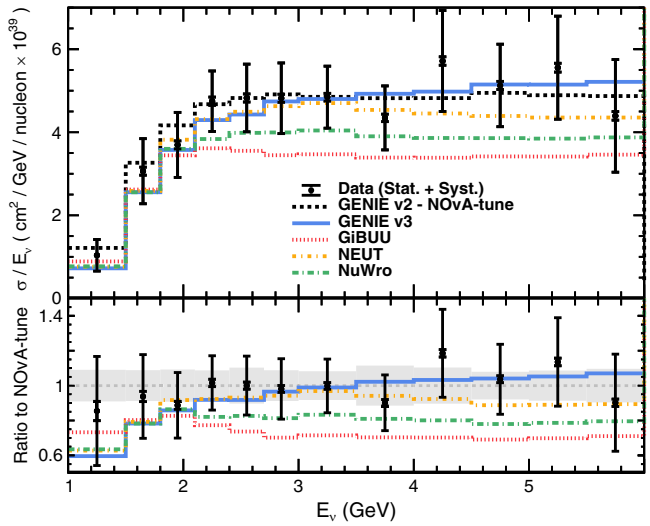

FIG. 4. Top: The differential cross section vs E_ν. Bottom: Comparisons as a ratio to the NOvA-tune prediction. The gray band represents the normalization uncertainty from the neutrino flux prediction. The data are presented showing statistical and total uncertainties.

and the differential cross section vs Q^2 shown in Fig. 5. All results are calculated from data using unfolding and efficiency corrections derived from the NOvA tune. The one-dimensional results apply the phase space restrictions in (1), without any restriction on the derived quantities of E_ν or $Q^2\{=2E_\nu[E_e-(P_e\cos\theta_e)]-m_e^2\}$. E_ν is reconstructed using a quadratic function determined from a 2D fit to the simulated electron and hadronic calorimetric energy [38]. The result is extracted with unfolding and efficiency corrections in E_ν or Q^2.

The extracted cross sections are compared to predictions from several generators: GENIE (NOvA-tune, v2.12.2, and

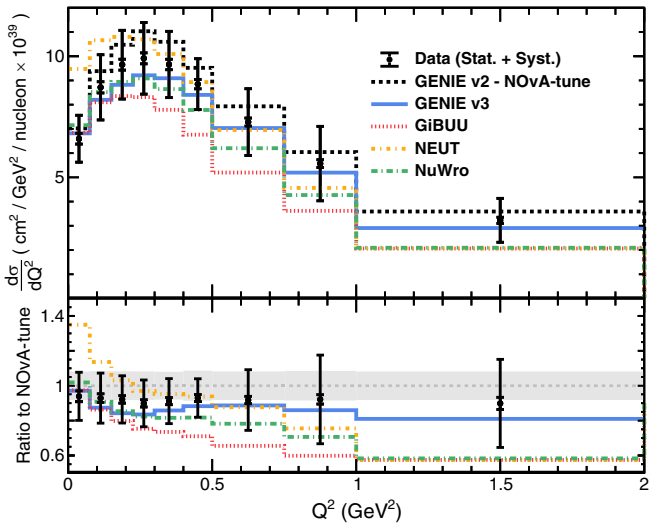

FIG. 5. Top: the differential cross section vs Q^2. Bottom: as in Fig. 4, but for Q^2.

v3.00.06 with a global configuration N18_10j_02_11a), NuWro 2019 [13], GiBUU 2019 [11], and NEUT 5.4.0 [12]. Table II summarizes χ^2 values for each model compared to data with a full treatment of bin-to-bin correlations. The values show no model is consistently favored across the ensemble of measurements.

Though the GiBUU and NuWro predictions have normalizations systematically lower than the data in Figs. 3–5 (15% and 10%, respectively) their χ^2s in Table II are comparable to other models' due to the phenomenon of Peelle's Pertinent Puzzle (PPP) [39,40]. PPP arises when the dominant uncertainty of a result is from highly correlated normalization uncertainties, like the flux uncertainty in Table I. Under these circumstances, the best-fitting model as reckoned by χ^2 can be well outside the data points. Disagreements with the GENIE predictions are dominated by the discrepancy in the $E_e > 4.75$ GeV bin and its correlations with other bins. When this bin is excluded from the calculation, the χ^2's for the GENIE predictions approach those of the NuWro and GiBUU predictions. NEUT shows slight disagreement throughout that angular slice, predicting a softer energy spectrum than is observed in data.

In E_ν comparisons NuWro and GiBUU plateau at a lower total cross section than the data as described above. The differential cross section vs Q^2 shows preference toward the NOvA-tune and GENIE v3 predictions. NEUT predicts a softer Q^2 distribution than seen in data, while GiBUU and NuWro accurately predict the low Q^2 behavior but tension is seen at high Q^2. The gray band in Fig. 5 shows the size of the flux-related normalization uncertainties, which illustrates that differences seen between data and the generators are not consistent with an overall change in the cross-section normalization.

This Letter presents the first measurement of the inclusive charged-current double-differential electron-neutrino cross section vs electron energy and angle, using the NOvA ND. This provides new information concerning directly observable final-state electron kinematics necessary for neutrino energy estimation and efficiency correction in ν_e appearance measurements. Measured cross sections are shown compared to multiple versions of GENIE, and to GiBUU, NEUT, and NuWro event generators, in the neutrino energy range from 1 to 6 GeV. The models show general agreement

TABLE II. χ^2 calculated for each model presented in Figs. 3–5 compared to data. Degrees of freedom are 17, 12, and 9 for the double-differential, E_ν, and Q^2 results, respectively.

Generator	$d^2\sigma/d\cos\theta_e dE_e$	$\sigma(E_\nu)$	$d\sigma/dQ^2$
GENIE v2—NOvA-tune	24.1	13.4	1.3
GENIE v2.12.2	24.3	14.3	19.6
GENIE v3.00.06	27.4	21.6	3.4
GiBUU 2019	17.5	16.0	14.7
NEUT 5.4.0	25.1	16.9	45.0
NuWro 2019	18.7	15.3	10.0

with the data in the two-dimensional phase space as well as various levels of success in the neutrino energy and Q^2 measurements. Disagreements are seen in both overall normalization across all reported measurements and with certain shape differences, primarily seen in Q^2. The data related to this measurement and systematic covariance matrices can be found at [41].

This document was prepared by the NOvA Collaboration using the resources of the Fermi National Accelerator Laboratory (Fermilab), a U.S. Department of Energy, Office of Science, HEP User Facility. Fermilab is managed by Fermi Research Alliance, LLC (FRA), acting under Contract No. DE-AC02-07CH11359. This work was supported by the U.S. Department of Energy; the U.S. National Science Foundation; the Department of Science and Technology, India; the European Research Council; the MSMT CR, GA UK, Czech Republic; the RAS, MSHE, and RFBR, Russia; CNPq and FAPEG, Brazil; UKRI, STFC and the Royal Society, United Kingdom; and the state and University of Minnesota. We are grateful for the contributions of the staffs of the University of Minnesota at the Ash River Laboratory, and of Fermilab.

[1] M. A. Acero *et al.* (NOvA Collaboration), Phys. Rev. Lett. **123**, 151803 (2019).
[2] K. Abe *et al.* (The T2K Collaboration), Phys. Rev. D **103**, L011101 (2021).
[3] B. Abi *et al.* (DUNE Collaboration), J. Instrum. **15**, T08008 (2020).
[4] M. Yokoyama (Hyper-Kamiokande Proto Collaboration), in Prospects in Neutrino Physics (2017), arXiv:1705.00306.
[5] M. Day and K. S. McFarland, Phys. Rev. D **86**, 053003 (2012).
[6] J. Blietschau *et al.* (Gargamelle Collaboration), Nucl. Phys. **B133**, 205 (1978).
[7] K. Abe *et al.* (T2K Collaboration), Phys. Rev. Lett. **113**, 241803 (2014).
[8] Tomohiro Abe, Motoko Fujiwara, Junji Hisano, and Yutaro Shoji (T2K Collaboration), J. High Energy Phys. 10 (2020) 114.
[9] J. Wolcott *et al.* (MINERvA Collaboration), Phys. Rev. Lett. **116**, 081802 (2016).
[10] C. Andreopoulos *et al.*, Nucl. Instrum. Methods Phys. Res., Sect. A **614**, 87 (2010).
[11] O. Lalakulich, K. Gallmeister, and U. Mosel, J. Phys. Conf. Ser. **408**, 012053 (2013).
[12] Y. Hayato, Acta Phys. Pol. B **40**, 2477 (2009), https://inspirehep.net/literature/844435.
[13] T. Golan, J. Sobczyk, and J. Zmuda, Nucl. Phys. B, Proc. Suppl. **229–232**, 499 (2012).
[14] M. Martini, M. Ericson, G. Chanfray, and J. Marteau, Phys. Rev. C **80**, 065501 (2009).
[15] J. Nieves, I. R. Simo, and M. J. VicenteVacas, Phys. Rev. C **83**, 045501 (2011).
[16] G. D. Megias, J. E. Amaro, M. B. Barbaro, J. A. Caballero, T. W. Donnelly, and I. R. Simo, Phys. Rev. D **94**, 093004 (2016).
[17] T. Van Cuyck, N. Jachowicz, R. Gonzalez-Jimenez, J. Ryckebusch, and N. VanDessel, Phys. Rev. C **95**, 054611 (2017).
[18] P. Adamson *et al.*, Nucl. Instrum. Methods Phys. Res., Sect. A **806**, 279 (2016).
[19] S. Mufson, B. Baugh, C. Bower, T. E. Coan, J. Cooper, L. Corwin, J. A. Karty, P. Mason, M. D. Messier, A. Pla-Dalmau, and M. Proudfoot, Nucl. Instrum. Methods Phys. Res., Sect. A **799**, 1 (2015).
[20] S. Agostinelli *et al.*, Nucl. Instrum. Methods Phys. Res., Sect. A **506**, 250 (2003).
[21] L. Aliaga *et al.* (MINERvA Collaboration), Phys. Rev. D **94**, 092005 (2016); **95**, 039903 (2017).
[22] M. Acero *et al.* (NOvA Collaboration), Eur. Phys. J. C **80**, 1119 (2020).
[23] A. S. Meyer, M. Betancourt, R. Gran, and R. J. Hill, Phys. Rev. D **93**, 113015 (2016).
[24] T. Katori, AIP Conf. Proc. **1663**, 030001 (2015).
[25] A. Aurisano, C. Backhouse, R. Hatcher, N. Mayer, J. Musser, R. Patterson, R. Schroeter, and A. Sousa, J. Phys. Conf. Ser. **664**, 072002 (2015).
[26] N. Anfimov, A. Antoshkin, A. Aurisano, O. Samoylov, and A. Sotnikov, J. Instrum. **15**, C06066 (2020).
[27] M. Ester *et al.*, in *Proceedings of the Second International Conference on Knowledge Discovery and Data Mining, KDD'96* (AAAI Press, USA, 1996), pp. 226–231.
[28] M. Baird, J. Bian, M. Messier, E. Niner, D. Rocco, and K. Sachdev, J. Phys. Conf. Ser. **664**, 072035 (2015).
[29] J. C. Dunn, J. Cybern. **3**, 32 (1973).
[30] A. Hoecker *et al.*, arXiv:physics/0703039.
[31] F. James and M. Roos, Comput. Phys. Commun. **10**, 343 (1975).
[32] G. D'Agostini, Nucl. Instrum. Methods Phys. Res., Sect. A **362**, 487 (1995).
[33] T. Adye, in *Proceedings of the PHYSTAT 2011 Workshop* (CERN, Geneva, 2011), pp. 313–318.
[34] W. T. Eadie *et al.*, *Statistical Methods in Experimental Physics*, 1st ed. (North-Holland, Amsterdam, 1971).
[35] B. Z. Kopeliovich, I. Schmidt, and M. Siddikov, Phys. Rev. D **85**, 073003 (2012).
[36] B. Z. Kopeliovich, Neutrino production of pions off nuclei version 1.0, http://atlas.fis.utfsm.cl/np/index.html.
[37] M. A. Acero *et al.*, Measurement of the double-differential muon-neutrino charged-current inclusive cross section in the nova near detector, arXiv:2109.12220.
[38] F. Psihas, Measurement of long baseline neutrino oscillations and improvements from deep learning, Ph.D. thesis, Indiana University, 2018, https://www.osti.gov/biblio/1437288.
[39] D. L. Smith, *Probability, Statistics, and Data Uncertainties in Nuclear Science and Technology* (American Nuclear Society, La Grange Park, 1991).
[40] R. Frühwirth, D. Neudecker, and H. Leeb, EPJ Web Conf. **27**, 00008 (2012).
[41] M. Acero *et al.* (NOvA Collaboration), NOvA Data Release Webpage, https://novaexperiment.fnal.gov/data-releases/ (2022).